Journal of Quantitative Spectroscopy & Radiative Transfer 217 (2018) 29–34

Contents lists available at ScienceDirect

Journal of Quantitative Spectroscopy & Radiative Transfer

journal homepage: www.elsevier.com/locate/jqsrt

A new linelist for the $A^3\Pi$–$X^3\Sigma^-$ transition of the NH free radical

Anton M. Fernando[a,*], Peter F. Bernath[a,b], James N. Hodges[b], Thomas Masseron[c,d]

[a] Department of Physics, Old Dominion University, Norfolk, VA 23529, USA
[b] Department of Chemistry and Biochemistry, Old Dominion University, Norfolk, VA 23529, USA
[c] Instituto de AstrofÃsica de Canarias, La Laguna, Tenerife E-38205, Spain
[d] Departmento de AstrofÃsica, Universidad de La Laguna, La Laguna, Tenerife E-38205, Spain

ARTICLE INFO

Article history:
Received 16 February 2018
Revised 21 May 2018
Accepted 21 May 2018
Available online 23 May 2018

Keywords:
NH
Linelist
A–X transition
Einstein A values
Lifetimes
Herman–Wallis effect

ABSTRACT

A new linelist for the $A^3\Pi$–$X^3\Sigma^-$ electronic transition of NH has been prepared using line positions from the literature and calculated line intensities. High level *ab initio* calculations were performed with the MOLPRO program to obtain the *A–X* transition dipole moment function. Potential energy curves and line strengths were calculated with Le Roy's RKR1 and LEVEL programs. Line intensities and Einstein A values were calculated with Western's PGOPHER program after converting the Hund's case (b) output of LEVEL to Hund's case (a) input needed for PGOPHER. The Herman–Wallis effect is included in the Einstein A calculations of the bands for the levels with $v' = 0 - 2$ and $v'' = 0 - 6$.

1. Introduction

The NH radical plays an important role in astrophysics. The bands of the $A^3\Pi$–$X^3\Sigma^-$ transition were first detected in a laboratory spectrum in 1893 [1]. The first astronomical observation of the NH *A–X* system was made in the spectrum of the Sun [2]. In 1940, the *A–X* system of NH was detected in the Comet Cunningham [3]. The $A^3\Pi$–$X^3\Sigma^-$ transition of NH was first recorded in the interstellar medium in 1991, towards the stars HD 27778 and HD 24398 and again in 1997 towards the star HD 149757 [4,5]. In 2009, interstellar NH abundances were calculated using the lines of the *A–X* system recorded towards the stars HD 149757, HD 170740, HD 154368 and HD 169454 [6].

NH is also frequently detected in the infrared spectra of cool stars. The infrared vibration-rotation lines of NH in oxygen-rich M giant stars, including α Orionis, were analyzed in order to obtain nitrogen abundances [7,8]. In 1986, nitrogen abundances for six additional stars were calculated using the observed infrared spectra [9].

In stellar atmospheres, although the formation of N-bearing molecules is strongly dominated by N_2 [10], molecular transitions are an excellent indicator of N abundances. Despite its dependence on carbon abundance, the CN molecule in the red and near infrared spectral regions is preferentially used by stellar spectroscopists because a higher stellar signal is obtained.

With the advent of a new generation of spectrographs such as UVES mounted on the VLT [11], the observation of the short wavelength region of the spectrum has become accessible. Indeed, the *A–X* transition of NH has been observed in stars and notably in metal-poor stars [12,13]. Spite et al. [13] noticed a systematic discrepancy in the N abundance derived from NH compared to the value derived from CN. They suspected that the NH *A–X* linelist needed revision, which we provide in the present paper.

The assignment of the 0–0 and 1–1 bands of the *A–X* system was carried out in the 1930s from emission spectra [14]. In 1959, the 0–0 and 1–0 bands were recorded in absorption [15] and in 1966 and 1970 several additional bands were analyzed [16,17]. In 1986, the *A–X* system of NH was measured with a precision of ± 0.0002 cm^{-1} for the 0–0, 1–1, 2–2, 0–1, 1–2, 1–0 and 2–1 bands [18]. These measurements improved on the previously available line positions by more than two orders of magnitude. The vibration-rotation lines in the infrared region were re-analyzed using solar spectra as well as IR laboratory spectra [19,20].

The $A^3\Pi$–$X^3\Sigma^-$ system recorded by Brazier et al. [18] used a copper hollow cathode discharge of helium with added nitrogen and hydrogen. The *A–X* spectrum was recorded with the Fourier transform spectrometer associated with the McMath-Pierce Solar Telescope of the National Solar Observatory at Kitt Peak [18].

* Corresponding author.
E-mail address: afern018@odu.edu (A.M. Fernando).

https://doi.org/10.1016/j.jqsrt.2018.05.021
0022-4073/

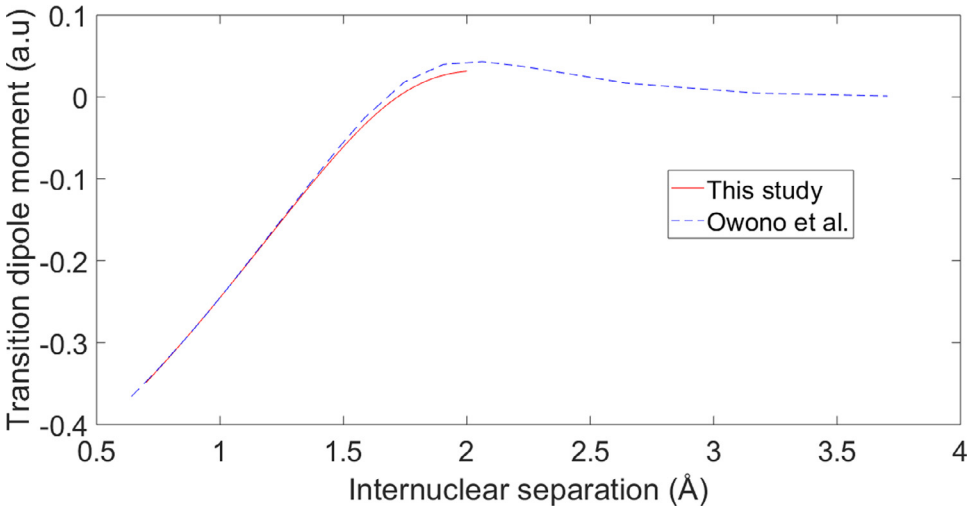

Fig. 1. Calculated transition dipole moment function for NH $A^3\Pi$–$X^3\Sigma^-$ compared with the TDMF calculated by Owono et al. [29].

2. Method

2.1. Experimental data

The spectroscopic constants for $A^3\Pi$ and $X^3\Sigma^-$ states were obtained from Ram and Bernath [20] based on Brazier et al. [18] for the A–X transition and Ram et al. [19] for the infrared vibration-rotation and pure rotation lines. The X state constants from Ram and Bernath [20] were also used by Brooke et al. [21] for the vibration-rotation line intensity analysis. The Brazier et al. A–X spectrum [18] will be used for comparison with our new linelist. We do not include ^{15}NH in our analysis because it was not detected in the spectrum of Brazier et al. [18].

2.2. Transition dipole moment function calculations

MOLPRO 2012 [22] was used to perform *ab initio* calculations of the transition dipole moment function of the $A^3\Pi$–$X^3\Sigma^-$ transition. To calculate the transition moment, the multireference configuration interaction (MRCI) method was used with the aug-cc-pwCV5Z basis set. The wavefunctions utilized for the MRCI calculations were obtained from state-averaged CASSCF (Complete Active Space Self-Consistent Field) calculations with the $A^3\Pi$ and $X^3\Sigma^-$ states having equal weights. All the electrons were included in the correlation treatment. The active space included the 2-5a_1, 1-2b_1, 1-2b_2 and 1a_2 orbitals in the C_{2v} point symmetry group used by MOLPRO. The TDMF (transition dipole moment function) points were calculated for internuclear distances between 0.7 Å and 2 Å in steps of 0.02 Å as expectation values. The calculated TDMF is provided as supplementary data.

2.3. Potential functions

The potential energy curves of the $A^3\Pi$ and $X^3\Sigma^-$ states were calculated employing Le Roy's RKR1 program [23]. The RKR1 program produces classical turning points of the potential energy curves using the first order semi-classical Rydberg–Klein–Rees procedure. The RKR1 program requires vibrational and rotational constants as the input in order to perform the calculations. The molecular constants required for the $X^3\Sigma^-$ state were obtained from Ram and Bernath [20] and for the $A^3\Pi$ state from Brazier et al. [18] (Table 1). The dissociation energy for the ground state ($D_0 = 27,409 \pm 13\,\mathrm{cm}^{-1}$) was obtained using the enthalpy of formation of N, H and NH at 0 K from the Active Thermochemical Tables [24] and for the excited state using a thermochemical cycle ($D_0 = 16,874 \pm 13\,\mathrm{cm}^{-1}$). The error in the dissociation energy was calculated by propagation of the errors in the enthalpies given in the tables.

Table 1
Equilibrium constants for $A^3\Pi$ and $X^3\Sigma^-$ States of NH (cm^{-1}).

Constant	$X^3\Sigma^-$	$A^3\Pi$
D_e	29,030	18,465.5
T_e	–	29,790.5
ω_e	3282.220(15)	3231.70
$\omega_e x_e$	78.513(15)	98.48
$\omega_e y_e$	0.1341(61)	–
$\omega_e z_e$	−0.0066(11)	–
B_e	16.667704(29)	16.681963(8)
α_e	0.649670(91)	0.712880(35)
γ_e	−0.001674(71)	−0.016160
δ_e	−0.000067(25)	–
ϵ_e	−0.0000633(24)	–

2.4. Transition dipole moment matrix elements and the "Herman–Wallis effect"

The calculated potential energy curves (Fig. 2) were used as input for Le Roy's LEVEL program [25]. The LEVEL program generates vibrational wavefunctions by solving the 1-D Schrödinger equation and then uses them with a specified transition dipole moment function (TDMF) to calculate transition dipole moment matrix elements (TDMMEs). LEVEL does not include electron spin in its calculations which corresponds to Hund's case (b). In LEVEL the total angular momentum quantum number J ($\vec{J} = \vec{N} + \vec{S}$) is actually the quantum number N (total angular momentum except electron spin) [25]. The matrix elements provided by LEVEL include the rotational dependence that originates from the J-dependent centrifugal term in the 1-D vibrational Schrödinger equation (i.e. the vibrational wavefunctions depend on J). These TDMMEs are transformed into Hund's case (a) using the method of Brooke et al. [21] and then input into Western's PGOPHER [26] to calculate the linelist.

When a diatomic molecule is rotating, it increases its bond length as a result of the centrifugal force [27]. Therefore the vibrational wavefunctions of the molecule change due to rotation and this affects the molecular properties. In particular, infrared line intensities can no longer be separated into a vibrational part times a Hönl-London factor [28]. This mechanical effect of the vibration-

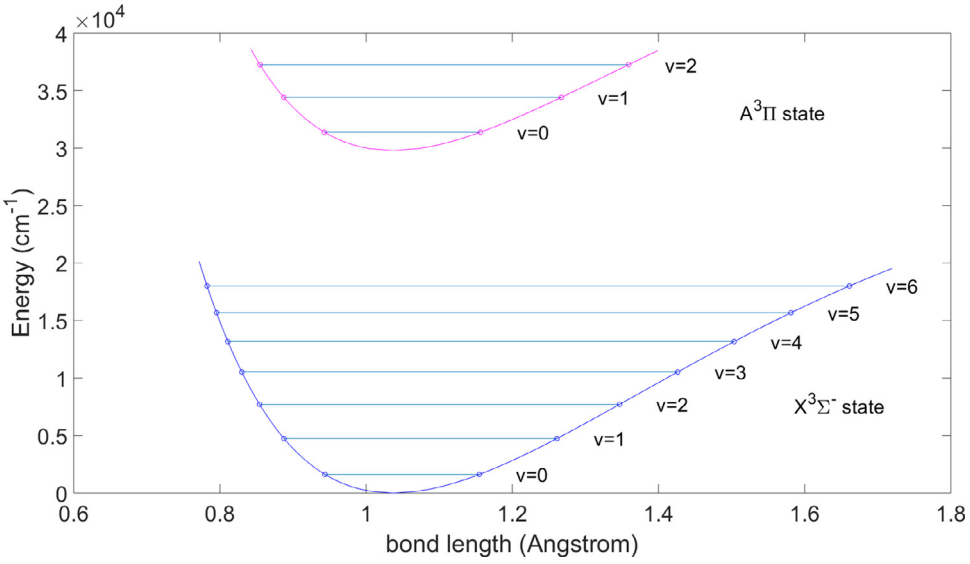

Fig. 2. Calculated RKR potential curves of the $A^3\Pi$ and $X^3\Sigma^-$ states for NH.

rotation interaction on line intensities is called the "Herman–Wallis effect" [27]. Einstein A calculations were done using PGOPHER including the *J*-dependent TDMMEs. PGOPHER calculates line intensities using the equations [28]:

$$A_{\eta' J' \longrightarrow \eta J} = \frac{16\pi^3 \nu^3 S_{\eta' J' \eta J}}{3\epsilon_0 hc^3 (2J'+1)} \quad \text{(SI Units)} \tag{1}$$

$$A_{\eta' J' \longrightarrow \eta J} = 3.13618932 \times 10^{-7} \frac{\tilde{\nu}^3 S_{\eta' J' \eta J}}{(2J'+1)}. \tag{2}$$

Line strength $S_{\eta' J' \eta J}$ in Eq. (2) is in debye squared, $A_{\eta' J' \longrightarrow \eta J}$ is in s^{-1} and $\tilde{\nu}$ is in cm^{-1}.

The calculated linelist is provided as supplementary data. All of the bands for $v' = 0$–2 and $v'' = 0$–6 are included for $\Delta v \leq 4$; 0–5, 0–6, 1–6 bands were not included as the Einstein A values are probably not reliable because of numerical problems in the LEVEL calculations. For each band, *J* was limited to about 5 *J* values beyond the highest observed value.

3. Results and discussion

3.1. Transition dipole moment function

The transition dipole moment function (TDMF) calculated in this study was compared with the TDMF available in the literature calculated by Owono et al. [29]. Owono et al. [29] carried out the calculations by using the aVTZ basis set and the orbitals needed for the configuration interaction (CI) were obtained by the CASSCF method. The CASSCF wavefunctions were then used for the MRSD-CI (multireference single and double excitation configuration interaction) routine to include electron correlation [29]. Our calculations used a larger basis set (aug-cc-pwCV5Z) and more extensive electron correlation than Owono et al. [29]. Our transition dipole moment function deviates from that of Owono et al. [29] for values greater than 1.5 Å, but in general, our TDMF agrees with the Owono et al. [29] TDMF (Fig. 1). (The polarity of the Owono et al. [29] TDMF was changed in order to compare with our TDMF.)

Our TDMF was also compared with the TDMF calculated by Song et al. [30] and they are in good agreement. (Since Song et al. [30] do not provide numerical points for the TDMF, the comparison was done with the published figure.)

Table 2
Comparison of the radiative lifetimes of the vibrational levels of the A state.

v'	τ (ns)	Ref.
0	388	This study
	449	[30] (Calc)
	453 ± 10	[35] (Exp)
	440 ± 15	[36] (Exp)
	390 ± 40	[37] (Exp)
1	436	This study
	484	[30] (Calc)
	488 ± 10	[35] (Exp)
	414 ± 6	[38] (Exp)
	390 ± 40	[37] (Exp)
	420 ± 35	[36] (Exp)
2	511	This study
	520	[30] (Calc)

3.2. Einstein A coefficients and lifetimes

The calculated lifetimes and Einstein A coefficients in this study were compared with experimental and theoretical values available in the literature as listed in Tables 2 and 3. A large Herman–Wallis effect was observed in the ground state as calculated by Brooke et al. [21]. In order to estimate the Herman–Wallis effect in the *A*–*X* transition, two sets of line strengths were calculated with and without including the Herman–Wallis effect. The line strengths without the Herman–Wallis effect were calculated with PGOPHER by using a single band strength (P(2) from the output of LEVEL) and the line strengths with the Herman–Wallis effect were calculated by using the *J*-dependent TDMMEs.

Since the experimental emission spectrum [18] does not have a well defined temperature, our line strengths cannot be compared directly with the observations. For comparison purposes, the ratio of ${}^rR_3(J'')$ and ${}^pP_3(J''+2)$ lines of the same upper state J' values were calculated, in order to cancel the effect of the excited state population in line intensities. These two sets of ratios were then compared with each other and then also with the ratios calculated from the experimental spectrum of Brazier et al. [18].

The ${}^rR_3(J'')/{}^pP_3(J''+2)$ ratios of the 0-0 vibrational band were calculated up to J'=25. For the lower J' values, the percentage difference between the ${}^rR_3(J'')/{}^pP_3(J''+2)$ ratios calculated with and

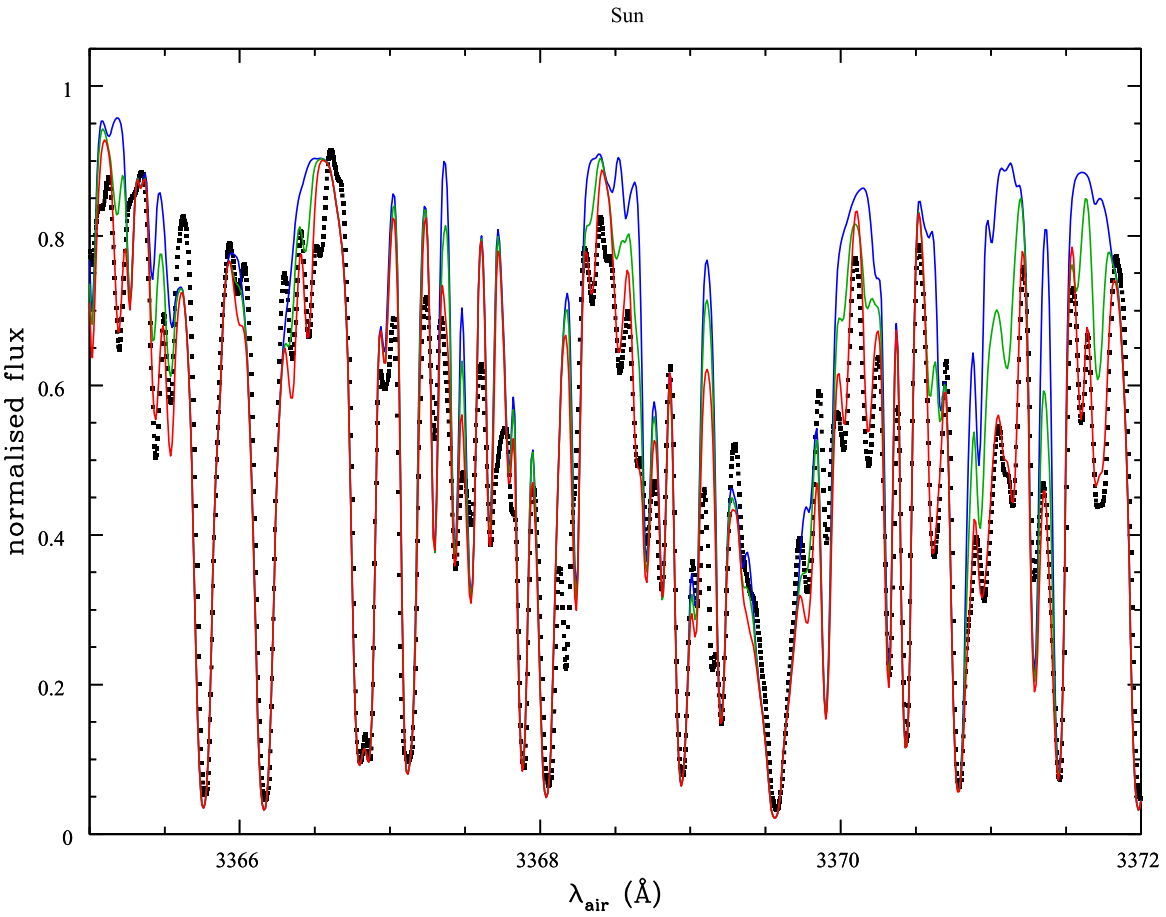

Fig. 3. Comparison between the observed spectrum of the Sun (black dotted line) and their respective syntheses with (red) and without (blue) the linelist presented in this work as well as the former linelist from Kurucz (http://kurucz.harvard.edu/molecules/) (green). (For interpretation of the references to color in this figure legend, the reader is referred to the web version of this article.)

Table 3
Einstein A coefficient comparison.

Band(A–X)	$A_{v'v''}$ ($\times 10^7 s^{-1}$)	Ref.
0–0	0.254	This study
	0.260	[29] (Calc)
	0.2522	[39] (Calc)
	0.226	[36] (Calc)
1–0	0.005870	This study
	0.005781	[29] (Calc)
	0.006425	[39] (Calc)
	0.007484	[40] (Calc)
1–1	0.218	This study
	0.226	[29] (Calc)
	0.2169	[39] (Calc)
	0.291	[41] (Calc)
2–0	0.00003	This study
	0.0001	[29] (Calc)
2–1	0.0139	This study
	0.0116	[29] (Calc)
2–2	0.181	This study
	0.193	[29] (Calc)
	0.220	[42] (Calc)

without including the Herman–Wallis effect is about 0.5% and for the higher J' values, the ratios are between 1% and 2.5%. In general, the percentage ratios measured from the observed [18] and the calculated spectra are also in good agreement (about 15% discrepancy) and the Herman–Wallis effect in the electronic transition is small.

3.3. Spectral validation

In order to validate the results, two observed astronomical spectra were used. In the Fig. 3, the observed spectrum of the solar photosphere is compared to a synthetic spectrum calculated with the new linelist. The spectra are from high resolution and high signal-to noise observations by Neckel [31]. There is very good agreement with the solar spectrum testifying to the high quality of our linelist.

While a solar N abundance of 7.78, as employed in this 1D-LTE synthesis, appears consistent with other N indicators [32], a comprehensive 3D model of the solar photosphere is required to confirm this value using our linelist.

In Fig. 4, a spectrum of the nitrogen-rich metal-poor star HD196944 obtained with the blue arm of the UVES spectrograph is presented. Concerning the overlaid synthesis, the parameters for this metal-poor star have been adopted from Masseron et al. [33]. In particular, the N abundance has been obtained by Masseron et al. [33] by using CN transitions. Fig. 4 demonstrates that there is now very good agreement with the N abundance obtained from the CN lines in contrast to the value obtained with the previous NH linelist. Therefore, we conclude that the problem of the N abundance discrepancy between CN and NH indicators as raised by Spite et al. [13] is now solved with our new NH linelist.

3.4. Lifetimes and Einstein A comparison

The lifetime of an excited rovibronic level depends on the radiative emission to all lower states and the non-radiative decay due

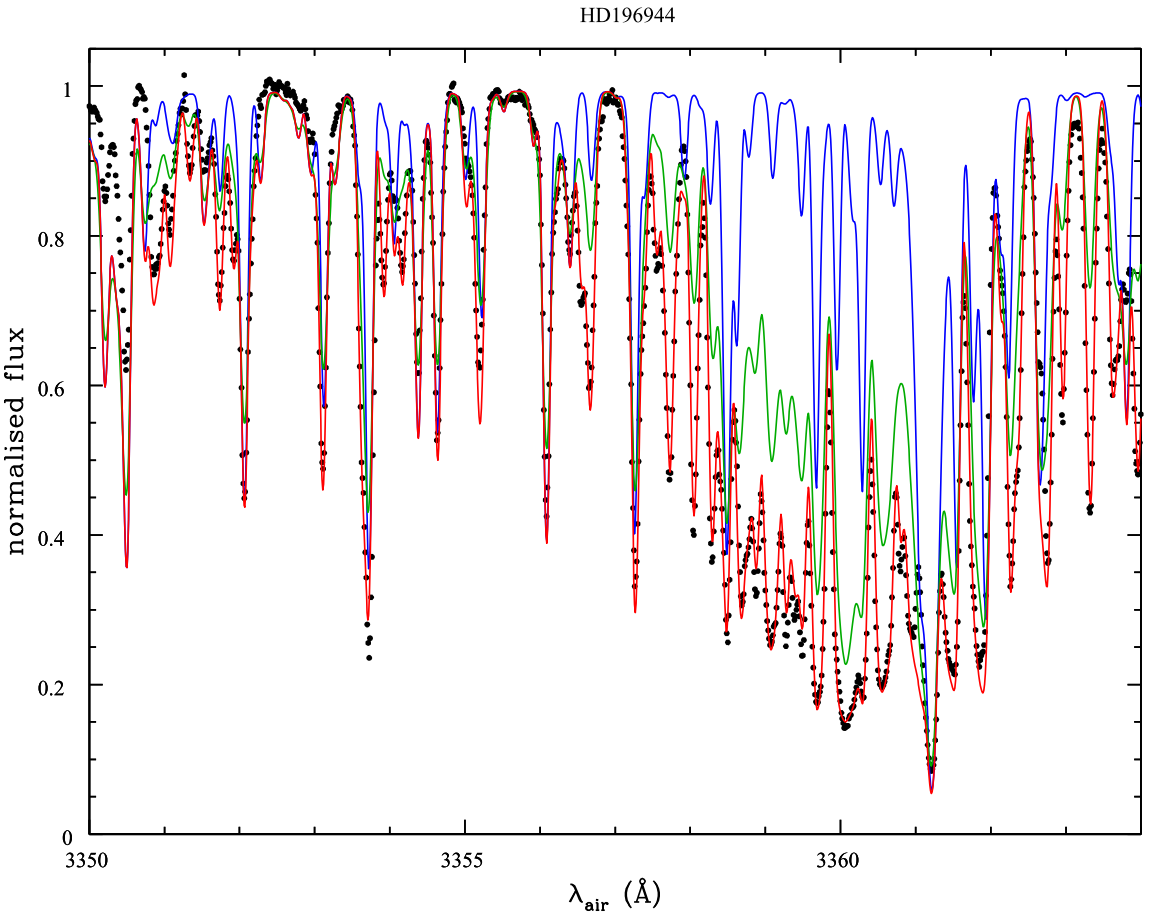

Fig. 4. Comparison between the observed stellar spectrum of the metal-poor star HD196944 (black dotted line) and their respective syntheses with (red) and without (blue) the linelist presented in this work as well as the former linelist from Kurucz (http://kurucz.harvard.edu/molecules/) (green). (For interpretation of the references to color in this figure legend, the reader is referred to the web version of this article.)

Table 4
A portion of the linelist.

v'	J'	N'	Sym'	v''	J''	N''	Sym''	Position (cm^{-1})	f-value	$A_{v'v''}$ (s^{-1})	Branch
0	0	1	e	0	1	0	e	29826.9444	0.0009454	1,683,060	$^{r}P_{31}(1)$
2	11	11	f	2	10	10	f	29826.6657	0.0016010	867,477	$^{r}R_{2}(10)$
1	5	5	f	1	5	4	e	29826.1839	0.0003161	187,576	$^{r}Q_{21}(5)$
1	5	5	f	1	4	4	f	29825.0871	0.0020780	1,008,750	$^{r}R_{2}(4)$
2	12	11	e	2	11	10	e	29822.8867	0.0016190	883,903	$^{r}R_{1}(11)$
2	3	4	e	2	2	1	e	29816.1540	0.0000003	137	$^{r}R_{31}(2)$
1	6	5	e	1	5	4	e	29814.7189	0.0023200	1,163,823	$^{r}R_{1}(5)$
2	4	5	f	2	4	3	e	29811.6183	0.0000045	2662	$^{s}Q_{31}(4)$
2	4	5	f	2	3	3	f	29810.6036	0.0000435	20,045	$^{s}R_{32}(3)$
2	9	10	e	2	10	9	e	29809.9762	0.0000005	295	$^{r}P_{31}(10)$
0	3	2	e	0	2	1	e	29809.8176	0.0034430	1,457,625	$^{r}R_{1}(2)$
2	9	10	e	2	8	9	e	29809.1619	0.0016770	889,531	$^{r}R_{3}(8)$
2	9	10	e	2	9	9	f	29808.6222	0.0000695	41,212	$^{r}Q_{32}(9)$
0	1	1	f	0	1	0	e	29807.2843	0.0027230	1,613,856	$^{r}Q_{21}(1)$
2	10	10	f	2	10	9	e	29806.4612	0.0000719	42,585	$^{r}Q_{21}(10)$
1	3	4	e	1	4	3	e	29805.1718	0.0000176	13,388	$^{r}P_{31}(4)$
2	10	10	f	2	9	9	f	29805.1072	0.0016290	873,561	$^{r}R_{2}(9)$
1	3	4	e	1	2	3	e	29805.0871	0.0022630	958,018	$^{r}R_{3}(2)$
1	3	4	e	1	3	3	f	29804.1443	0.0004592	272,098	$^{r}Q_{32}(3)$

to predissociation [30]. In this study, the lifetimes in the $A^3\Pi$ excited state were calculated without taking predissociation into account. But, in general, our lifetimes are in good agreement with the values available in the literature (Table 2). Einstein A values were calculated for several vibrational bands and compared with values available in the literature, and they are in agreement (Table 3).

It is difficult to estimate the error in the NH Einstein A values obtained by *ab initio* calculations except by analogy with similar calculations for a system such as OH^+ with more information. An error analysis was carried out by Hodges et al. [34] for the $A^3\Pi$–$X^3\Sigma^-$ system of isoelectronic OH^+ and, based in part on astronomical observations, and the error was estimated to be about 10%. We can expect a similar error for the NH A–X system as well.

The experimental lifetimes in the literature for $v' = 0$ and 1 differ by significant amounts (Table 3). It is not clear which values

should be used to calibrate the line intensities so we recommend that our values, based on theory alone, be used.

4. Conclusion

A new linelist for the NH *A*–*X* transition has been generated. The line intensities were obtained with a dipole moment function calculated *ab initio* with a large basis set and with extensive electron correlation. The calculated line intensities included the Herman–Wallis effect. In contrast to the infrared bands, the Herman–Wallis effect is small for the *A*–*X* transition. Two astronomical spectra were used for the validation of the results and the calculated spectra are in good agreement with the observed spectra. The Einstein A values and lifetimes were compared with values available in the literature and they are generally in good agreement.

(A portion of the linelist is given in the Table 4. The complete linelist is provided as an ascii supplementary data file. The linelist includes *e*/*f* parity, the quantum numbers *J, N* and *v* for each state, line positions, oscillator strengths and Einstein A values.)

Acknowledgments

We thank Dror Bittner for the help with the *ab initio* dipole moment calculations. We acknowledge support provided by NASA laboratory astrophysics program and the Spanish Ministry of Economy and Competitiveness (MINECO) under the grants AYA201458082-P and AYA-2017-88254-P.

Supplementary material

Supplementary material associated with this article can be found, in the online version, at doi: 10.1016/j.jqsrt.2018.05.021.

References

[1] Eder JM. Contributions to spectral analysis. Denkschr Wien Akad 1893;60:1–24.
[2] Fowler A, Gregory CCL. The ultra-violet band of ammonia and its occurrence in the solar spectrum. Philos Trans Royal Soc A 1919;218(561–569):351–72.
[3] Swings P, Elvey CT, Babcock W. The spectrum of Comet Cunningham, 1940c. Astrophys J 1941;94:320.
[4] Meyer D, Roth K. Discovery of interstellar NH. Astrophys J 1991;376:L49–52.
[5] Crawford IA, Williams D. Detection of interstellar NH towards ζ Ophiuchi by means of ultra−high−resolution spectroscopy. Mon Notices Royal Astron Soc 1997;291(3):L53–6.
[6] Weselak T, Galazutdinov GA, Beletsky Y, Kreowski J. Interstellar NH molecule in translucent sightlines. Mon Notices Royal Astron Soc 2009;400(1):392–7.
[7] Lambert DL, Brown JA, Hinkle KH, Johnson HR. Carbon, nitrogen and oxygen abundances in Betelgeuse. Astrophys J 1984;284(3).
[8] Aoki W, Tsuji T. High resolution infrared spectroscopy of CN and NH lines: nitrogen abundance in oxygen-rich giants through K to late M. Astron Astrophys 1997;328.
[9] Smith VV, Lambert DL. The chemical composition of Red Giants. II. Helium burning and the s-process in the MS and S stars. Astrophys J 1986;311.
[10] Tsuji T. Molecular abundance in stellar atmospheres. Ann Tokyo Astron Observatory 1964;9:1–110.
[11] Dekker H, D'Odorico S, Kaufer A, Delabre B, Kotzlowski H. Design, construction, and performance of UVES, the echelle spectrograph for the UT2 Kueyen Telescope at the ESO Paranal Observatory. Proc SPIE 2000;4008:534–45. doi:10.1117/12.395512.
[12] Sneden C. The nitrogen abundance of the very metal-poor star HD 122563. Astrophys J 1973;184:839–49.
[13] Spite M, Cayrel R, Plez B, Hill V, Spite F, Depagne E, et al. First stars VI - abundances of C, N, O, Li, and mixing in extremely metal-poor giants. Galactic evolution of the light elements. Astron Astrophys 2005;430:655–68. astro-ph/0409536.
[14] Funke GW. Das absorptions spektrum des NH. Zeitschrift für Physik 1936;101(1):104–12.
[15] Dixon RN. The 0-0 and 1-0 bands of the $A^3\Pi - X^3\Sigma^-$ system of NH. Can J Phys 1959;37(10):1171–86.
[16] Murai T, Shimauchi M. Rotational distortions of $^3\Pi$ states applied to NH molecule. Sci Light (Tokyo) 1966;15:48–67.
[17] Malicet J, Brion J, Guenebaut H. Contribution to the spectroscopic study of the transition $A^3\Pi - X^3\Sigma^-$ of the NH radical. J Chim Phys 1970;67:25–30.
[18] Brazier C, Ram R, Bernath P. Fourier transform spectroscopy of the $A^3\Pi - X^3\Sigma^-$ transition of NH. J Mol Spectrosc 1986;120(4):381–402.
[19] Ram RS, Bernath PF, Hinkle KH. Infrared emission spectroscopy of NH: Comparison of a cryogenic echelle spectrograph with a Fourier transform spectrometer. J Chem Phys 1999;110(12):5557–63.
[20] Ram R, Bernath P. Revised molecular constants and term values for the $A^3\Pi$ and $X^3\Sigma^-$ states of NH. J Mol Spectrosc 2010;260(2):115–19.
[21] Brooke JSA, Bernath PF, Western CM. Improved line strengths of rovibrational and rotational transitions within the $X^3\Sigma^-$ ground state of NH. J Chem Phys 2015;143(2):026101. doi:10.1063/1.4923422.
[22] Werner H, Knowles PJ, Knizia G, Manby F, Schütz M. Molpro: a general-purpose quantum chemistry program package. Wiley Interdiscip Rev 2012;2(2):242–53.
[23] Le Roy RJ. RKR1: a computer program implementing the first-order RKR method for determining diatomic molecule potential energy functions. J Quant Spectrosc Radiat Transf 2017;186:158–66.
[24] Ruscic B. Active thermochemical tables: sequential bond dissociation enthalpies of methane, ethane, and methanol and the related thermochemistry. J Phys Chem A 2015;119(28):7810–37.
[25] Le Roy RJ. LEVEL: a computer program for solving the radial Schrödinger equation for bound and quasi-bound levels. J Quant Spectrosc Radiat Transf 2017;186:167–78.
[26] Western CM. PGOPHER: a program for simulating rotational, vibrational and electronic spectra. J Quant Spectrosc Radiat Transf 2017;186:221–42.
[27] Herman R, Wallis RF. Influence of vibration-rotation interaction on line intensities in vibration-rotation bands of diatomic molecules. J Chem Phys 1955;23(4):637–46.
[28] Bernath PF. Spectra of Atoms and Molecules. 3rd ed. Oxford University Press; 2016. ISBN 978-0-19-938257-6.
[29] Owono LCO, Abdallah DB, Jaidane N, Lakhdar ZB. Theoretical radiative properties between states of the triplet manifold of NH radical. J Chem Phys 2008;128(8):084309.
[30] Song Z, Shi D, Sun J, Zhu Z. Accurate spectroscopic calculations of the 12 Λ-S and 25 Ω states of the NH radical including the spin-orbit coupling effect. Comput Theor Chem 2016;1093(5):81–90.
[31] Neckel H. Announcement. Sol Phys 1999;184:421–2.
[32] Asplund M, Grevesse N, Sauval AJ, Scott P. The chemical composition of the Sun. Annu Rev Astron Astrophys 2009;47:481–522. 0909.0948. doi:10.1146/annurev.astro.46.060407.145222.
[33] Masseron T, Johnson J, Plez B, Van Eck S, Primas F, Goriely S, et al. A holistic approach to carbon-enhanced metal-poor stars. Astron Astrophys 2010;509:A93. doi:10.1051/0004-6361/200911744.
[34] Hodges JN, Bittner DM, Bernath PF. Improved ultraviolet and infrared oscillator strengths for OH^+. Astrophys J 2018;855(1):21.
[35] Gustafsson O, Kindvall G, Larsson M, Olsson B, Sigray P. An experimental and theoretical investigation of the radiative properties of the $A^3\Pi$ state of NH. Chem Phys Lett 1987;138(2):185–94.
[36] Fairchild PW, Smith GP, Crosley DR, Jeffries JB. Lifetimes and transition probabilities for NH ($A^3\Pi - X^3\Sigma^-$). Chem Phys Lett 1984;107(2):181–6.
[37] Hawkins WG, Houston PL. Hydrazine photochemistry induced by an argon fluoride excimer laser. J Phys Chem 1982;86(5):704–9.
[38] Smith WH, Brzozowski J, Erman P. Lifetime studies of the NH molecule: new predissociations, the dissociation energy, and interstellar diatomic recombination. J Chem Phys 1976;64(11):4628–33.
[39] Yarkony DR. On the electronic structure of the NH radical. The fine structure splitting of the $X^3\Sigma^-$ state and the spin forbidden $(b^1\Sigma^+, a^1\Delta) \rightarrow X^3\Sigma^-$, and the spin allowed $A^3\Pi - X^3\Sigma^-$ and $c^1\Pi \rightarrow (b^1\Sigma^+, a^1\Delta)$, radiative transitions. J Chem Phys 1989;91(8):4745–57.
[40] Sing PD, Gruenwald RB. The photodissociation lifetimes of the NH radical in comets. Astron Astrophys 1987;178:277–82.
[41] Lents J. An evaluation of molecular constants and transition probabilities for the NH free radical. J Quant Spectrosc Radiat Transf 1973;13(4):297–310.
[42] Smith W, Liszt H. Franck-Condon factors and absolute oscillator strengths for NH, SiH, S_2 and SO. J Quant Spectrosc Radiat Transf 1971;11(1):45–54.